RSC Advances

ROYAL SOCIETY OF CHEMISTRY

www.rsc.org/advances

First-principles Analysis of Seven Novel Phases of Phosphorene with Chirality

Jian-Rui Feng [1] and Gui-Chang Wang [1,2,*]

[1] Department of Chemistry, Key Laboratory of Advanced Energy Materials Chemistry (Ministry of Education), Nankai University, Tianjin 300071, P. R. China;

[2] State Key Laboratory of Coal Conversion, Institute of Coal Chemistry, Chinese Academy of Sciences, Taiyuan, 030001, P. R. China)

*Corresponding author: Gui-Chang Wang. E-mail: wangguichang@nankai.edu.cn

Telephone: +86-22-23503824 (O) Fax: +86-22-23502458

ABSTRACT

In this work, seven novel phases of phosphorene were predicted to be existent by first-principles calculations, including six kinds of enantiomers corresponding to three kinds of structures with chirality. It is the first time to involve chirality into two dimensional(2D) phosphorus. Poisson ratios are investigated and show normal behavior rather than negative one of monolayer or bulk black phosphorus, due to non-puckered structures. Phase transformations of these enantiomers are studied and it exhibits possibility of transformations between them because of low energy barriers, which open doors to possible applications of shape memory device. This work may inspire new ideas of developing novel applications based on 2D phosphorus nanomaterials.

KEYWORDS

Phosphorene; Nanometerials; Charility; Poisson ratio; Phase transformation

1. INTRODUCTION

Nanomaterials are investigated widely since graphene[1] was discovered. Hence carbon based structures[2,3] overflowed as the pioneer of nanoscale. After that, more development of research was made about two-dimensional boron nitride,[4,5] an isoelectronic counterpart of graphene. Progress were also made in noncarbon class of 2D elemental materials such as silicene,[6] germanene,[7] stanene,[8] phosphorene[9] and arsenene[10]. Transition metal dichalcogenides[11,12] was focused by researchers in recent years, which makes 2D family to be much diversified. In these popular area of 2D nanomaterials, phosphorenes possess many interesting properties such as negative Poisson ratio,[13,14] sensitivity of strain,[15] potential photocatalystic performance,[16] gas sensor[17] and anisotropic intrinsic lattice thermal conductivity.[18] In this work, chirality is first introduced into 2D phosphorus, which may inspire more works to develop this unique property for potential applications.

Most recently, many trials of developing new structure of phosphorene were adopted. Monolayered blue phosphorus (β-P),[19] γ-P and δ-P[20,21] were predicted by Zhu with a method of Density Functional Theory (DFT). Polymorphs of phosphorene with square (ε-P, ζ-P) and pentagon (η-P, θ-P) units[22] were proofed to be stable by BOMD (Born-Oppenheimer molecular dynamics) simulation and computation of lattice vibration spectra. Red phosphorene[23] was designed by analogy of black phosphorene and blue phosphorene. These works made phosphorus to be more fascinating for nanomaterial science.

Similar method was adopted to design new structures from other elements such as porous boron nitride (PBN),[24] which was designed as an analogue of porous graphene[25] and inorganic graphenylene (IGP),[26,27] which was verified to be existent as an analogue of biphenylene carbon (BPC).[28,29] It is mainly because 2D nano structures are similar in geometry conformation that method of analogy is feasible in predicting new phase. Hence it is possible to design new structures of blue phosphorene by means of analogue of binary elemental 2D structures such as hexagonal BN.

In previous reports,[26] by molecular dynamic simulation, by removing H atoms of PBN, an analogue of porous graphene, it will spontaneously transfer to a new structure, which named inorganic graphenylene (IGP), a structure similar to BPC. Interestingly, it is feasible to find new structures in 2D phosphorene by replacing the corresponding atoms in PBN and IGP. In this work, the two kinds of atoms in PBN and IGP are substituted by upper P atom and lower P atom, respectively. Vibration spectrum and BOMD were confirmed its stability. In addition, it is different from absolutely one atom layered BN that chirality exists in two atom layered phosphorus based 2D materials although they are only monolayer.

2. CALCULATION METHOD AND MODELS

In this work, simulations are based on density functional theory (DFT). Vienna ab initio simulation package (VASP)[30] was implemented to optimize structures and investigate properties. Interaction of ion-electron is depicted by projector augmented waves (PAW)[31] when the function of Perdew, Burke and Ernzerhof (PBE)[32] based on generalized gradient approximation (GGA) was adopted to describe the exchange and correlation potential. We set the cut off energy to 400eV in all calculations. To build 2D structure, a vacuum slab of approximate 20 Å was adopted. A 7×7×1 Γ-centered Monkhorst-Pack[33] k-point grid was used for sampling of the Brillouin zone of structure optimization and a 15×15×1 Γ-centered Monkhorst-Pack k-point grid was adopted for band structure calculation. The threshold of convergence was set to 1×10^{-4} eV and 0.01 eV/Å for self-consistent field (SCF) and ion-step, respectively. All the BOMD simulations were carried out using an NVT ensemble with a 1.0 fs time step and a 5 ps duration.

3. RESULTS AND DISCISSION

3.1 Structure and Stability of Porous Phosphorene, IGP-P and DHPP

There are three kinds of chemical bonds in porous phosphorene, including P-P bonds inner hexagonal cycles, P-P bonds connecting neighbor hexagonal cycles and P-H bonds. The optimized geometry structure and band structure of porous phosphorene is shown in Figure 1 (b). The lattice parameters of porous phosphorene are 9.83 Å for a and b, 90° for α and β, and 120° for γ. The indirect band gap of porous phosphorene is 2.30 eV, with the lowest point of CBM (conduction band minimum) locating at G and highest point of VBM (valence band maximum) locating at M. To confirm the correctness of the calculations, the lattice parameters and band structure of monolayered blue phosphorene are calculated (see Figure 1 (a)). It is 3.28 Å and 1.94 eV for modulation of lattice vectors and band gap in our calculation, respectively, which agrees with previous work.[19]

To find other new structures, we substituted these two kinds of atoms in IGP with upper P atoms and lower P atoms. This new phase of phosphorene was named inorganic graphenylene based on phosphorus (IGP-P), whose structure and band structure is shown in Figure 1 (c). There are three kinds of bonds in IGP, including P-P bonds in 4, 6-membered rings, respectively, and in both 4 and 6-membered rings. Lattice parameters of IGP-P are 8.91 Å for a and b, 90° for α and β, and 120° for γ. The indirect band gap of porous phosphorene is 1.89 eV, with the highest point of CBM locating at G and lowest point of VBM locating at K.

It is interesting to wonder whether it will spontaneously transfer to another phase when the H atoms of porous phosphorene was removed. Therefore, a BOMD simulation was adopted and resulted in a new structure, which we named dehydro porous phosphorene (DHPP), rather than IGP-P. The movie of BOMD could be approached in Supporting Information. There are 3, 4, 5-membered ring in a unit cell of DHPP. The reason that porous phosphorene doesn't transfer to IGP-P when H atoms were removed is that it is more favorable in energy to stay in DHPP phase. The cohesive energy is given in Table 1. Cohesive energy represents the energy that would be required to decompose a structure into isolated atoms. A more negative cohesive energy indicated a more stable structure. The formula to calculate cohesive energy is $E_c = E_{sys} - \sum n_x E_x$, where E_c, E_{sys}, n_x and E_x present for cohesive energy, energy of a system, number of x atoms and energy of one x atom. Hence it could be seen that all the structures may be stable with respect to thermodynamical stability. The blue phosphorene shows the cohesive energy of -3.47 eV, where there is no significant difference compared with new structures in this work. It should be noted that there are no sense to compare blue phosphorene with porous phosphorene because they are made of different elemental atoms while comparing blue phosphorene with IGP-P, DHPP and DHPP-2 makes sense. As for application, transformation between porous phosphorene and DHPP by removing hydrogen atoms indicates it may be a good idea to develop porous phosphorene as hydrogen storage materials.[34]

The lattice parameters of DHPP are 9.45 Å for a and b, 90° for α and β, and 120° for γ. A direct band gap of 1.55 eV at gamma point, which will be favor to develop it as photocatalyst and materials used for photoelectric conversion without involving energy consumption by phonon. Furthermore, we built another structure similar to DHPP and named it DHPP-2. It has different lattice from other structures. The lattice parameters are 10.41 Å and 7.81 Å for a and b, 90° for α and β, and 120° for γ. And it has an indirect band gap of 1.70 eV with the highest point of CBM located between G and K and lowest point of VBM locating at G.

For more detail informations about electronic properties of these structures, partial density of states (PDOS) were calculated as plotted in Figure 2. For porous phosphorene, H atoms contribute at CBM but rarely at VBM while density of states from P atoms contribute both VBM and CBM. For different quantum number l, p orbitals contributes the most of shallow levels while s orbitals rival at deep levels lower than 6 eV (vs. Fermi level). This phenomena that appears in all the four structures is in accordance with general quantum mechanics. Hence it is p orbitals of P atoms that contribute the VBM and CBM mostly in IGP-P, DHPP and DHPP-2. Band gaps read from PDOS are consistent with what read from band structures, although Gaussian algorithm was used for smearing which mades the curves smooth.

To study the vibration spectrum of these phosphorus allotropes, we use PHONOPY package[35] to analysis the phonon dispersion. The phonon dispersion spectrums of porous phosphorene, IGP-P and DHPP are shown in Figure 3. Besides, there are no significant imaginary frequency of these three phases, which indicates they may be stable and possible to be synthesized experimentally. Since electronic energy based on DFT calculation is related to 0 K, and the entropy correction should be included in order to relate to the real conditions, so free energy results were used to predicate the thermodynamic stability further. Helmholtz free energy was plotted as Figure 3(e). Free energy F(T) as a function of temperature of blue phosphorene agrees with previous report.[36] Consideration of the zero point energy gives rise to a slightly higher ground state energy for these phases at 0 K. And it could be seen that blue phosphorene (as stable as black phosphorene with respect to free energy[36]) is stable than all the other phases while F(T) of DHPP is lower than IGP-P and DHPP-2 at whole scale of temperature. It should be noted that comparing F(T) of porous phosphorene with other phases makes no sense because it includes different kinds of atoms when other phases only contain phosphorus atoms. Meanwhile, BOMD simulations at 700 K was performed and showed that these four structures are still intact after 5 ps and the whole frames were vibrating regularly. The movies of these BOMD simulations could be seen in Supporting Information.

3.2 Chirality of IGP-P DHPP and DHPP-2

Similar as binary elemental 2D materials, projection of blue phosphorene in z direction looks like a honeycomb. However, phosphorene is not absolutely one atom layered structure. There are two atom layers in monolayered phosphorene, so it is possible to involve chirality into systems of phosphorus based 2D structures. Our calculations concluded that chirality exists in IGP-P, DHPP and DHPP-2 and each phase has two kinds of enantiomers. The structures of enantiomers could be seen in Figure 4. We named these enantiomers with R and S as suffix. It is easy to identify an R or S enantiomer when the 4-membered ring is ascertained. If the two upper atoms in 4-membered ring are at upper left and bottom right from projection at z direction, it is an S enantiomer. If the lower atoms in 4-membered ring are at upper left and bottom right from projection at z direction, it is an R enantiomer. In fact, no matter how an enantiomer is rotated, this method to identify them is correct.

When chirality is considered, new application such as chirality catalysis, molecular self-assembly and polarized optics will be feasible in the future. Many previous works were conducted to utilize chirality of nanomaterials as a promised application.[37,38] As for chemical properties, it is significant that chirality presents an important role. To adsorption and separate different enantiomers of molecules, it is possible to

prepare these novel nanomaterials as functional resin. By modifying functional groups based on intrinsic charility of them, chiral catalysis may be achieve, for reactions of biochemical molecules including drugs and imaging agents, considering good compatibility of phosphorus in biochemistry. However, as for physical properties, currently the cohesive energy and band gap of two kinds of enantiomers are the same. So in this work, all the calculations are based on S enantiomers.

To emphasize the importance of their chirality, adsorption of chiral molecules on IGP-P-S was adopted for example. There are only one position of P atom in IGP-P-S and around a P atom there in turn exists 12, 4 and 6-membered ring clockwise. Hence each neighboring P atom of this P is different after we picked it. When enantiomers of molecules with chirality were adsorbed on this P atom, the interaction of substrate and three different ligands of the molecule is different. It is mostly Van der Waals force that contributes the difference and DFT-D3 correction[39,40] was adopted. So three kinds of molecules containing different number of atoms were tested. It is all known the bigger molecule is, the stronger Van der Waals force effects. As for the smallest molecule which only have five atoms, CHFClBr shows the smallest difference between its enantiomers. In contrast, glutamic acid shows biggest effect of chiral adsorption. It concludes that this kind of chiral materials may show selective adsorption of chiral molecules, which would be useful application. Detail data could be seen in Supporting Information.

3.3 Poisson Ratio of Porous Phosphorene, IGP-P and DHPP

To study the Poisson ratio of porous BP, IGP-P and DHPP, we calculated the strain along different directions at the same time, which method was adopted in a early work.[13,14] For calculating Poisson ratio, a square lattice was adopted. The transformational matrix of lattice vector is present as $\mathrm{M_t} = \begin{pmatrix} 1 & 0 & 0 \\ 1 & 2 & 0 \\ 0 & 0 & 1 \end{pmatrix}$. The vectors matrix after redefinition is obtained as $\begin{pmatrix} a_2 \\ b_2 \\ c_2 \end{pmatrix} = \mathrm{M_t} \begin{pmatrix} a_1 \\ b_1 \\ c_1 \end{pmatrix}$, where a_2,b_2,c_2 are for vectors after redefinition and a_1,b_1,c_1 are for vectors before redefinition. The redefined lattice are shown in Figure 5 (c) and (f), corresponding to IGP-P and DHPP.

We set strain along x and y direction in a range of -0.02 to 0.02 and a interval of 0.004, where date points could be see in Figure 5 as black dots. Strain energy is define as $\mathrm{E_s} = \mathrm{E_{x,\,y}} - \mathrm{E_{0,0}}$,where E_s, $E_{x,y}$ and $E_{0,0}$ present for stain energy, total energy of system when strain is adopted and total energy of system when no strain is adopted at two direction. The relationship of E_s, ε_x and ε_y is fitted in polynomial equation as

$E_S = a\varepsilon_x^2 + b\varepsilon_y^2 + c\varepsilon_x\varepsilon_y$, in which a, b and c are fitting parameters. The detail number of a,b and c could be seen in table 2. Stress along x(y)direction was calculated by formulation $\sigma_{x(y)} = V_0^{-1}\partial E_S/\partial\varepsilon_{x(y)}$, where V_0 is a constant as equilibrium volume. Uniaxial deformations along the x and y directions are indicated by dashed lines shown in Figure 5, which are denoted by $\sigma_x = 0$ and $\sigma_y = 0$, respectively. The corresponding Poisson's ratios are evaluated as $\nu_y = c/2a$ and $\nu_x = c/2b$, where ν_y and ν_x are defined as $\nu_y = -\varepsilon_x/\varepsilon_y$ and $\nu_x = -\varepsilon_y/\varepsilon_x$, respectively. The same method was adopted in an earlier report[14] and we successfully repeated results of it.

The Poisson ratios calculated are 0.379 (0.159) and 0.340 (0.208) for ν_y and ν_x for IGP-P (DHPP), respectively. It seems that Poisson ratios of IGP-P are larger than DHPP in both two in-plane directions. This phenomenon is mainly due to the cell volume of DHPP is larger than IGP-P, which makes force of atoms in DHPP lattice less than IGP-P when uniaxial strain adopted. Hence there are less influence on lattice deformation in another direction.

Then strain along z direction are calculated and plot in Figure 5 (b) and (e) for IGP-P and DHPP, respectively. Previous work[14] shows that both bulk and monolayered black phosphorus exhibit negative Poisson's ratios along its armchair direction in response to perpendicular uniaxial strains. However, in this work it is not the same. Under uniaxial strain along the x(y) direction, strain along z direction is increased (reduced) as the sheet is compressed (stretched), in which a positive strain indicates stretching and negative strain indicates compressing. It is different from the existence of a negative Poisson's ratio in black phosphorene. It is the structure that properties depend on. To be specific, the puckered structure of black phosphorene doesn't exist in blue phosphorene, where puckered structure means that when you look at the structure from top of black phosphorene, the lower atoms would be blocked by upper atoms. However, this phenomenon doesn't appear in blue one. Hence it concludes that IGP-P and DHPP exhibit normal Poisson ratio's behavior in response to all direction oriented uniaxial deformations.

3.4 Phase Transformation of enantiomers of IGP-P and DHPP

The phase transformations of different kinds of structures were investigated in previous research.[19,20,22] It is interesting that whether these new phases in this work are possible to transform to each other or not. For DHPP and IGP-P, their cell shapes are the same while their cell volumes are different. Actually, the cell volume could be presented as lattice constant |a| for a hexagonal lattice. So we plot energy of each phase when constant |a| varies in Figure 6 (a). It seems that IGP-P can be more stable than DHPP at relatively smaller cell volume, which could be approached by decrease pressure. Hence

transformation from DHPP to IGP-P under higher pressure is feasible by their energy dependence on cell volume.

Transition path of enantiomers of IGP-P and DHPP was also studied in this work. A method of generalized solid-state nudged elastic band (GSS-NEB)[41-43] was adopted to find energy barrier of their transformation. It is unlikely that the IGP-P-S transforms to IGP-P-R directly while it is easy for enantiomers of DHPP to be transformed within each other. If an enantiomer of IGP-P is willing to transform to another, the transition path is as follows. At first, transform to DHPP with the same chirality. Then, transform to DHPP with the different chirality. At last, transform to IGP-P with the different chirality. Path of transformations are shown in Figure 6 (b) for DHPP-S to IGP-P-S and (c) for DHPP-S to DHPP-R, respectively. It is bilateral symmetric for plotted transformation path of different enantiomers of the same phase while it is bilateral asymmetric for plotted transformation path of different phases with the same chirality. The calculated potential barrier of IGP-P-S to DHPP-S(IGP-P-R to DHPP-R),DHPP-S to DHPP-R(DHPP-R to DHPP-S) is 0.066 eV/atom and 0.077 eV/atom, respectively. Such small energy barrier indicates that it is possible to obtain racemic IGP-P and DHPP when the system absorbs enough energy from environment. It is reasonable expected that if some pure IGP-S was obtained, it would transform to mixture of IGP-P-S, IGP-P-R, DHPP-S and DHPP-R by suitable heating.

It is likely that GSS-NEB method underestimates the energy barrier, so it may be a little higher in reality. We also tested another method used in previous researches,[19,22] in which lattice constants of initial state was redefined to coincide with the lattice of the final state. The calculations show that there is no significant difference between these two methods due to the similar lattice configuration.

4. CONCLUSION AND PROSPECT

In this work, four new phases of phosphorene were predicted to be exist when three of them have a property of chirality and enantiomers. The transformations of them are investigated and it seems to be possible to obtain racemic production in certain conditions. Poisson ratio are found negative in z direction and it may inspire development of areas in energy store and mechanics. Their property of chirality is possible to be used as optical materials and chiral catalysis. Transformation between porous phosphorene and DHPP by removing hydrogen atoms indicates it may be a good application to develop porous phosphorene as hydrogen storage materials.

For experimental fabrication,[44] top-down methods and bottom-up methods are both possible to obtain these large-hole structures. When black phosphorus is cleaved by large-volume ions in solution

environments, the ions are embedded into layers of bulk. Hence the layers are separated by force of ions. In this procedure, defects of large hole may be generated. As for bottom-up methods, it depends on the substrates when chemical vapor deposition (CVD) is adopted. If specific substrates were used, these materials would be synthesized.

In addition, the catalysis activity of group of phosphorene is not thoroughly studied so far. The property of Lewis base makes phosphorene to be a likely good catalyst in some specified reactions. Involving chirality, it will be more interesting in chiral catalysis by phosphorus based nanomaterials. More experimental and theoretic study may stimulate the potential of these novel materials.

Acknowledgements

This work was supported by the State Key Program of Natural Science of Tianjin (Grant No. 13JCZDJC26800), MOE Innovation Team (IRT13022) of China, the National Natural Science Foundation of China (Grants No. 142100, 21433008, 91545106), and the foundation of State Key Laboratory of Coal Conversion (Grant No. J15-16-908).

REFERENCES

1 K. S. Novoselov, A. K. Geim, S. V. Morozov, D. Jiang, Y. Zhang, S. V. Dubonos, I. V. Grigorieva and A. A. Firsov, Science, 2004, 306, 666-669.

2 H. Zhang, W. Ding and D. K. Aidun, Journal of Nanoscience and Nanotechnology, 2015, 15, 1660-1668.

3 H. Zhang, W. Ding, K. He and M. Li, Nanoscale Research Letters, 2010, 5, 1264-1271.

4 D. Pacile, J. C. Meyer, C. O. Girit and A. Zettl, Applied Physics Letters, 2008, 92.

5 X.-F. Zhou, X. Dong, A. R. Oganov, Q. Zhu, Y. Tian and H.-T. Wang, Physical Review Letters, 2014, 112.

6 P. De Padova, C. Quaresima, C. Ottaviani, P. M. Sheverdyaeva, P. Moras, C. Carbone, D. Topwal, B. Olivieri, A. Kara, H. Oughaddou, B. Aufray and G. Le Lay, Applied Physics Letters, 2010, 96.

7 Z. Ni, Q. Liu, K. Tang, J. Zheng, J. Zhou, R. Qin, Z. Gao, D. Yu and J. Lu, Nano Letters, 2012, 12, 113-118.

8 P. Tang, P. Chen, W. Cao, H. Huang, S. Cahangirov, L. Xian, Y. Xu, S.-C. Zhang, W. Duan and A. Rubio, Physical Review B, 2014, 90.

9 H. Liu, A. T. Neal, Z. Zhu, Z. Luo, X. Xu, D. Tomanek and P. D. Ye, Acs Nano, 2014, 8, 4033-4041.

10 S. Zhang, Z. Yan, Y. Li, Z. Chen and H. Zeng, Angewandte Chemie-International Edition, 2015, 54, 3112-3115.

11 P. K. Chow, E. Singh, B. C. Viana, J. Gao, J. Luo, J. Li, Z. Lin, A. L. Elias, Y. Shi, Z. Wang, M. Terrones and N. Koratkar, Acs Nano, 2015, 9, 3023-3031.

12 Y. Ding and B. Xiao, Rsc Advances, 2015, 5, 18391-18400.

13 J.-W. Jiang and H. S. Park, Nat. Commun., 2014, 5.

14 M. Elahi, K. Khaliji, S. M. Tabatabaei, M. Pourfath and R. Asgari, Physical Review B, 2015, 91.

15 R. Fei and L. Yang, Nano Letters, 2014, 14, 2884-2889.

16 B. Sa, Y.-L. Li, J. Qi, R. Ahuja and Z. Sun, Journal of Physical Chemistry C, 2014, 118, 26560-26568.

17 L. Kou, T. Frauenheim and C. Chen, Journal of Physical Chemistry Letters, 2014, 5, 2675-2681.

18 R. Fei, A. Faghaninia, R. Soklaski, J.-A. Yan, C. Lo and L. Yang, Nano Letters, 2014, 14, 6393-6399.

19 Z. Zhu and D. Tomanek, Physical Review Letters, 2014, 112.

20 J. Guan, Z. Zhu and D. Tomanek, Physical Review Letters, 2014, 113.
21 J. Guan, Z. Zhu and D. Tomanek, Acs Nano, 2014, 8, 12763-12768.
22 M. Wu, H. Fu, L. Zhou, K. Yao and X. C. Zeng, Nano Letters, 2015, 15, 3557-3562.
23 T. Zhao, C. Y. He, S. Y. Ma, K. W. Zhang, X. Y. Peng, G. F. Xie and J. X. Zhong, Journal of Physics-Condensed Matter, 2015, 27.
24 Y. Ding, Y. Wang, S. Shi and W. Tang, Journal of Physical Chemistry C, 2011, 115, 5334-5343.
25 P. Kuhn, A. Forget, D. Su, A. Thomas and M. Antonietti, Journal of the American Chemical Society, 2008, 130, 13333-13337.
26 E. Perim, R. Paupitz, P. A. S. Autreto and D. S. Galvao, Journal of Physical Chemistry C, 2014, 118, 23670-23674.
27 J. R. Feng and G. C. Wang, Computational Materials Science, 2016, 111, 366-373.
28 G. Brunetto, P. A. S. Autreto, L. D. Machado, B. I. Santos, R. P. B. dos Santos and D. S. Galvao, Journal of Physical Chemistry C, 2012, 116, 12810-12813.
29 Y. Li, D. Datta, Z. Li and V. B. Shenoy, Computational Materials Science, 2014, 83, 212-216.
30 G. Kresse and J. Furthmüller, Phys. Rev. B Condens. Matter Mater. Phys., 1996, 54, 11169-11186.
31 P. E. Blöchl, Physical Review B, 1994, 50, 17953-17979.
32 J. P. Perdew, K. Burke and M. Ernzerhof, Physical Review Letters, 1996, 77, 3865-3868.
33 H. J. Monkhorst and J. D. Pack, Physical Review B, 1976, 13, 5188-5192.
34 J. Luo, H.-B. Zhou, Y.-L. Liu, L.-J. Gui, S. Jin, Y. Zhang and G.-H. Lu, Journal of Physics-Condensed Matter, 2011, 23.
35 A. Togo, F. Oba and I. Tanaka, Phys. Rev. B Condens. Matter Mater. Phys., 2008, 78.
36. Y. Aierken, D. Cakir, C. Sevik and F. M. Peeters, Physical Review B, 2015, 92.
37 J. L. Zhang, T. C. Niu, A. T. S. Wee and W. Chen, Physical Chemistry Chemical Physics, 2013, 15, 12414-12427.
38 T. Chen, Q. Chen, X. Zhang, D. Wang and L.-J. Wan, Journal of the American Chemical Society, 2010, 132, 5598-+.
39 S. Grimme, J. Antony, S. Ehrlich and H. Krieg, J Chem Phys, 2010, 132.
40 S. Grimme, S. Ehrlich and L. Goerigk, J. Comput. Chem., 2011, 32, 1456-1465.
41 G. Henkelman, B. P. Uberuaga and H. Jonsson, J Chem Phys, 2000, 113, 9901-9904.
42 G. Henkelman and H. Jonsson, J Chem Phys, 2000, 113, 9978-9985.
43 D. Sheppard, P. Xiao, W. Chemelewski, D. D. Johnson and G. Henkelman, J Chem Phys, 2012, 136.
44 L. Kou, C. Chen and S. C. Smith, Journal of Physical Chemistry Letters, 2015, 6, 2794-2805.

TABLE 1. Lattice parameters, cohesive energy, cohesive energy (considering zero point energy) and band gap of blue phosphorene and four new phases

Structure	a (Å)	b (Å)	E_c (eV)	$E_{c,z}$ (eV)	E_g (eV)
Blue phosphorene	3.28		-3.47	-3.42	1.94
Porous phosphorene	9.83		-2.69	-2.58	2.30
IGP-P	8.91		-3.33	-3.28	1.89
DHPP	9.45		-3.34	-3.29	1.55
DHPP-2	10.42	7.81	-3.33	-3.28	1.70

TABLE 2. Fitting numbers and calculated Possion ratios of IGP-P and DHPP

Structure	a	b	c	v_y	v_x
IGP-P	174.22	194.61	132.21	0.379	0.340
DHPP	159.73	122.40	50.89	0.159	0.208

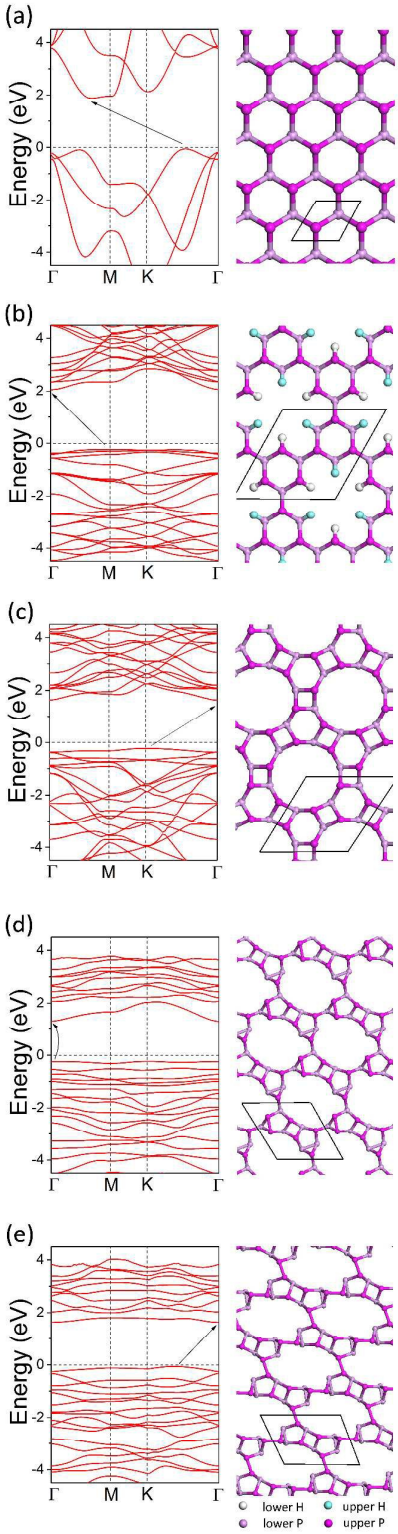

Figure 1. Geometric configurations and band structures of blue phosphorene and four new phases. Arrow indicates the highest point at VBM and lowest point at CBM. Upper position and lower position of atoms are denoted by deep colors and light colors, respectively. Unit cells are denoted by black box.

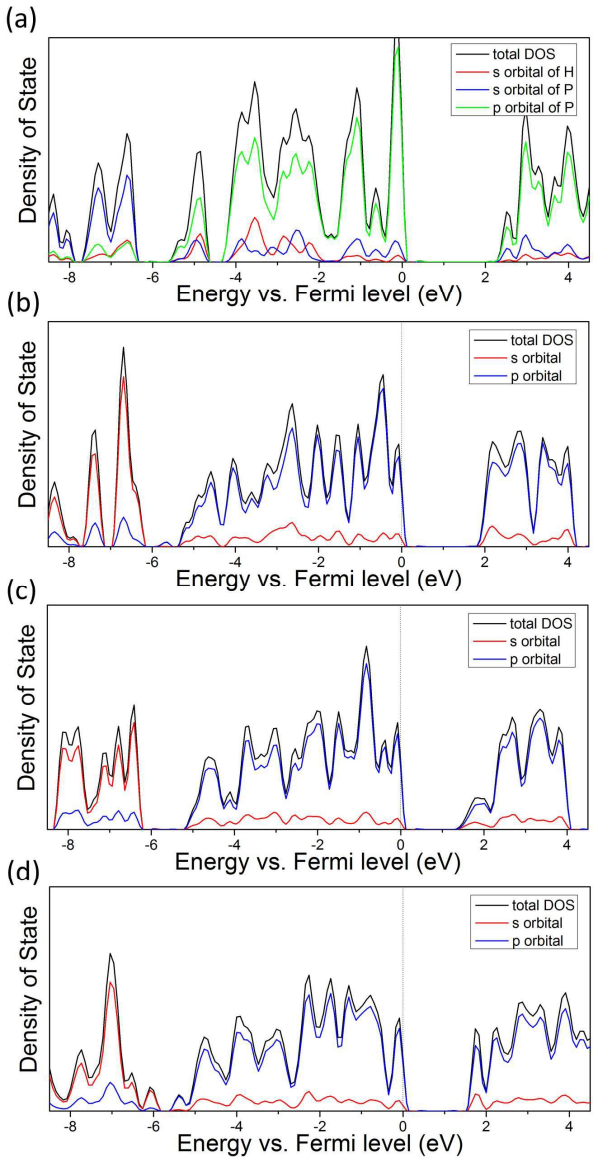

Figure 2. Partial density of states of porous phosphorene (a), IGP-P (b), DHPP (c) and DHPP-2 (d), in which contribution from different quantum number l and different kinds of atoms are separated.

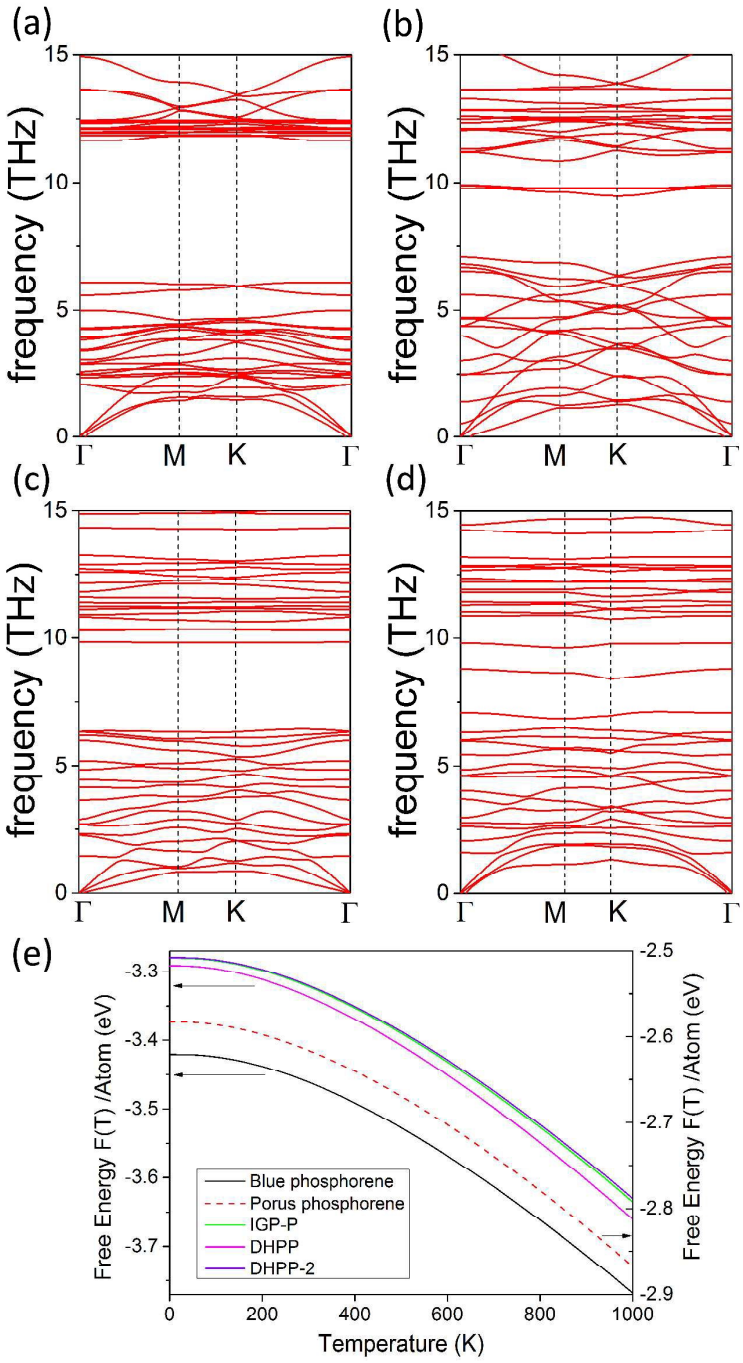

Figure 3. Phonon dispersion spectrums of (a) porous phosphorene, (b) IGP-P, (c) DHPP and (d) DHPP-2. (e) Helmholtz free energy F(T) as a function of temperature.

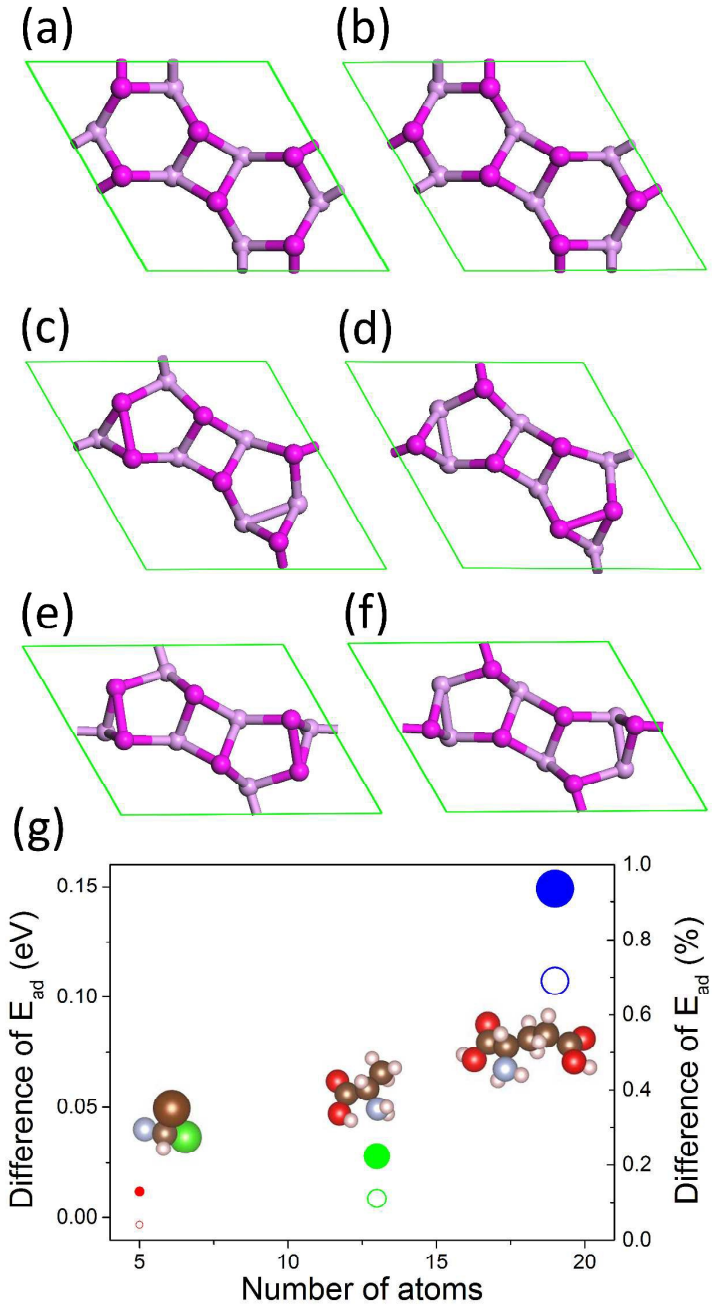

Figure 4. Enantiomers of IGP-P, DHPP and DHPP-2. (a) IGP-P-S (b) IGP-P-R (c) DHPP-S (d) DHPP-R (e) DHPP-2-S (f) DHPP-2-R.Upper position and lower position of atoms are denoted by deep colors and light colors, respectively. (g) Differences of adsorption energy corresponding to enantiomers of CHFClBr, alanine and glutamic acid adsorbed on IGP-P, in which solid circle relates to left axis and hollow circle relates to right axis.

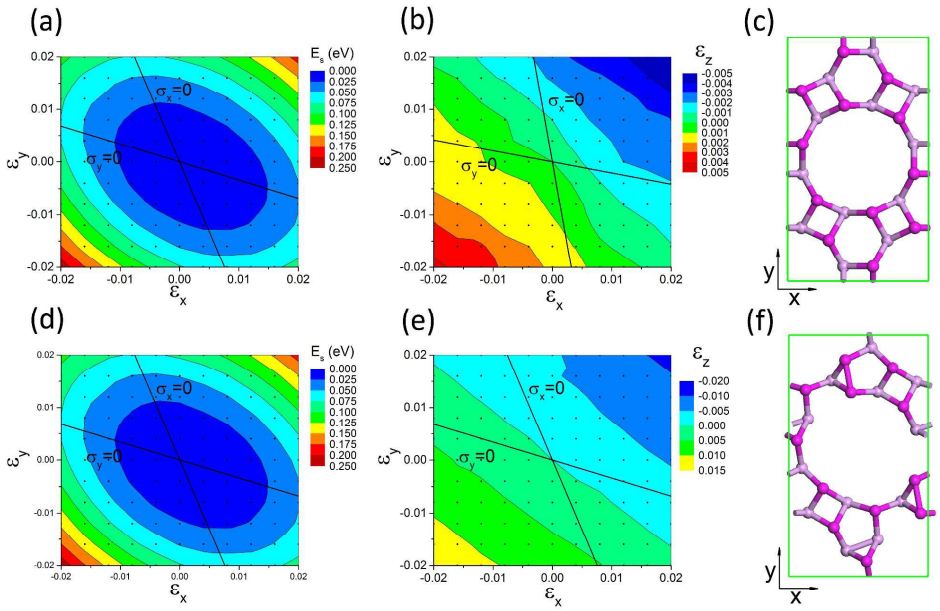

Figure 5. Surface plot of (ε_x, ε_y) and the corresponding strain energies of (a) IGP-P and (d) DHPP. Surface plot of (ε_x, ε_y) and the corresponding ε_z of (b) IGP-P and (e) DHPP. Redefined lattice adopted for Poisson ratio's calculation of (c) IGP-P and (f) DHPP.

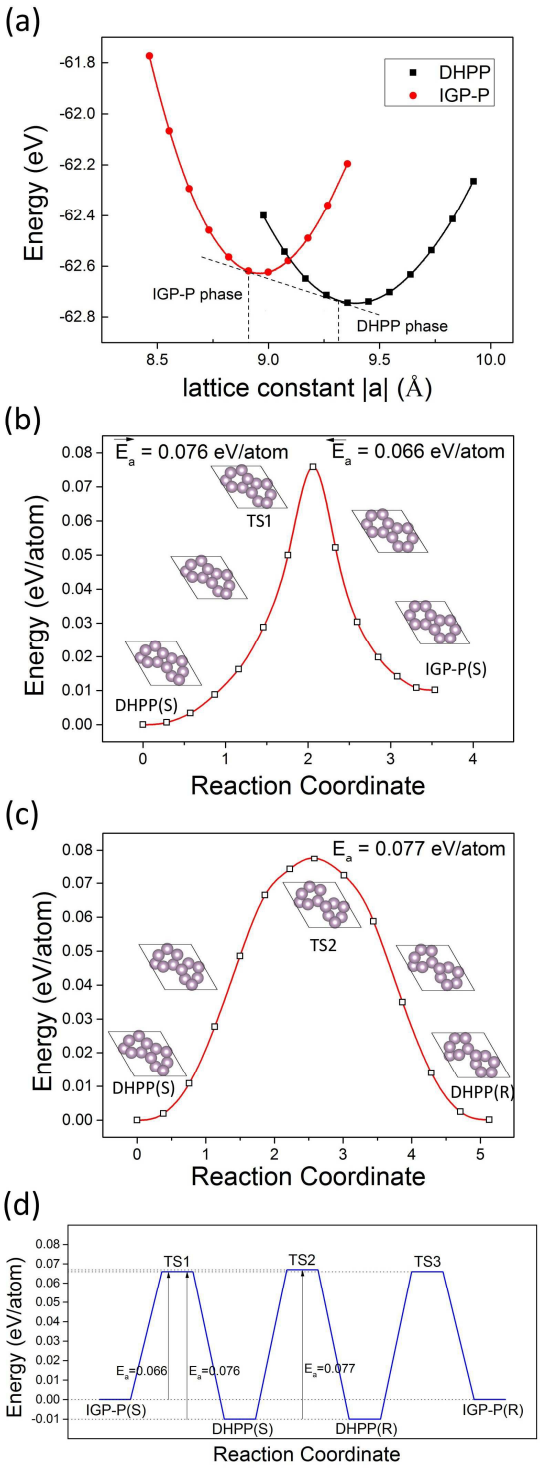

Figure 6. (a) Transformation from IGP-P to DHPP under external pressure, which is revealed to be feasible by their energy dependence on cell volume denoted by lattice constant |a|. (b) Transformation path and energy barrier from DHPP-S to IGP-P-S. (c) Transformation path and energy barrier between two enantiomers of DHPP. (c) Whole scale of transformation of enantiomers of IGP-P and DHPP, where E_a presents for activation energy of transformation.

Graphical abstract